symmetry

MDPI

Article

Propagation Prediction of Body Waves in Fluid-Saturated Soils with Flow-Independent Viscosity

Bo Wang [1,2,*], Xingyuan Zhang [1,2] and Bo Sun [1,2]

[1] School of Civil Engineering, Longdong University, Qingyang 745000, China; ldxyzhangxy@sina.com (X.Z.); ldxysunb@sina.com (B.S.)
[2] Gansu Province Gully Fixing and Tableland Protection Engineering Research Center, Longdong University, Qingyang 745000, China
* Correspondence: ldxywangb@sina.com

Abstract: A systematic study of wave theory in thermoviscoelastic soil is essential for engineering applications such as geophysical exploration. In the present work, the influences of flow-independent viscosity of the soil skeleton and the thermal effect on elastic waves are considered, and the propagation behaviors of body waves in thermoviscoelastic saturated soil are investigated. Firstly, the thermoviscoelastic dynamic coupling model of saturated soil were established by employing the Biot model, the generalized thermoelastic theory, and the Kelvin–Voigt linear viscoelastic model. Secondly, the dispersion equations of body waves in thermoviscoelastic saturated soil were theoretically derived with structural symmetry considered. Finally, the variations of wave velocity and the attenuation coefficient of the body waves with the thermophysical parameters are discussed. The results revealed that the enhancement of the relaxation time of soil caused an increase of wave velocity and the attenuation coefficient of P_1, P_2, and S waves, and a decrease of the wave velocity and attenuation coefficient of the thermal wave. Different ranges of the permeability coefficient and frequency have different effects on the P_1, P_2, and S waves. The variation of thermal conductivity and the phase-lags of heat flux and temperature gradient only affect the thermal wave.

Keywords: thermoviscoelasticity; saturated soil; body wave; wave velocity; attenuation coefficient

check for updates

Citation: Wang, B.; Zhang, X.; Sun, B. Propagation Prediction of Body Waves in Fluid-Saturated Soils with Flow-Independent Viscosity. *Symmetry* **2022**, *14*, 408. https://doi.org/10.3390/sym14020408

Academic Editor: Huaping Wang

Received: 25 January 2022
Accepted: 16 February 2022
Published: 18 February 2022

Publisher's Note: MDPI stays neutral with regard to jurisdictional claims in published maps and institutional affiliations.

Copyright: © 2022 by the authors. Licensee MDPI, Basel, Switzerland. This article is an open access article distributed under the terms and conditions of the Creative Commons Attribution (CC BY) license (https://creativecommons.org/licenses/by/4.0/).

1. Introduction

The nondestructive detection of industrial materials, such as mutiphase soil, oil reserves, pile testing, concrete testing, etc., are implemented on the basis of wave response, such as phase velocity, attenuation, and travel time. The propagation behaviors of the elastic wave in materials are not only dependent on the materials' elastic characteristics, but also the thermal and viscous characteristics. Therefore, it is of great engineering and theoretical significance to investigate the relationship of materials' thermoviscoelastic parameters and the propagation behaviors of the elastic wave.

Under an isothermal condition, there are generally two types of elastic waves present in the single-phase medium, namely, body waves and surface waves. Body waves, including compression and shear waves, propagate in unbounded domains. Surface waves, mainly for Rayleigh and Love waves, are identified as the superposition of body waves and propagate along the medium boundary. Therefore, the research of body waves propagation is a crucial basis for studying the other types of waves. When considering the influences of temperature change, there is a type of thermal wave in the single-phase medium besides compression, shear, and surface waves. Because the form of natural soil is generally biphase or even complex multiphase, researchers have carried out many related works on elastic wave propagation in multiphase media. Biot [1,2] first developed the dynamic equation of saturated poroelastic media filled with single-phase fluid, and successfully predicted that there are two compression waves, i.e., P_1 and P_2 waves, and one shear wave, i.e., S wave, in fluid-saturated poroelastic media, which has been validated by Plona [3] and

Berryman [4] through laboratory experiments. Therefore, the model developed by Biot laid the foundation for the dynamic analysis in biphase or even multiphase porous media. Since then, based on the Biot model, many researchers [5–24] carried out various related works on the propagation of elastic waves in saturated porous media.

In the process of interdisciplinary research, such as the petrochemical process and nuclear waste management, the thermal effect, such as temperature change, also has serious influence on the propagation of elastic waves, which is keenly noticed by researchers. Biot [25] first developed the thermoelastic coupling model of single-phase solid medium and predicted a kind of thermal wave propagating at infinite speed, which is contrary to the fact that the wave propagates at finite speed. Then, Lord and Shulman [26] modified the early thermoelastic coupling model of single-phase solid medium and predicted the finite wave velocity propagation of thermal wave. In subsequent studies, considering the polyphasy of natural soil, researchers macroscopically regard it as a kind of porous elastic medium with pores filled with fluids such as water, oil, or gas to construct the thermoelastic wave model in saturated soil. Youssef [27] considered a homogeneous, isotropic elastic body with a boundary filled by compressible ideal liquid and established a generalized thermoelastic theory. Following, Singh [22] developed a more complex thermoelastic coupling model of porous media; however, the meaning of some of the physical parameters were not sufficiently clear due to the complexity of the model. For the propagation of thermoelastic body waves in saturated soil, Liu et al. [28] developed a thermoelastic dynamic model for studying the spherical cavity's thermoelastic dynamic response in saturated porous medium under nontorsional loads. Recently, Zhou et al. [29] established a thermal-fluid-solid coupling elastic wave model for saturated porous media with clear physical parameters, and studied the evolution of Rayleigh wave velocity, whereas the non-Fourier heat conduction with single-phase lag model was adopted so that only the phase-lag of the temperature gradient influenced the wave characteristics.

Although many works have been carried out on the propagation characteristics of elastic/thermoelastic waves in saturated soils, most of which only consider the viscosity associated with the pore-fluid flow, i.e., the coupling effect between pore fluid and the solid skeleton. However, it is well known that the deformation of nature soils under the action of external force is apparently time dependent. That is, the viscoelasticity of the solid skeleton is associated with the flow-independent viscosity, which is likely to affect the propagation characteristics of elastic waves, but is mostly ignored in existing related literatures. Fortunately, the dependence of soil and structure responses on the viscoelasticity of the soil skeleton was established many years ago [30–32]. Naturally, it is necessary to establish a closer relationship between the propagation behavior of elastic waves and the flow-independent viscosity of the soil skeleton. The elastic constants of soil (i.e., the bulk modulus, the Lame constant, and shear modulus) should be related to the flow-independent viscosity by the relaxation time.

The present work simplifies the natural soil to a fluid-saturated porous medium, which consists of a soil particle composing the solid skeleton and liquid filling the pores between the skeleton. Considering the influences of the thermal effect and the flow-independent viscosity of natural soil, a thermoviscoelastic dynamic coupling model of fluid-saturated soil were established by employing the Biot model, the generalized thermoelastic theory, and the Kelvin–Voigt linear viscoelastic model, and the dispersion equations of the body waves were theoretically derived by employing the Helmholtz resolution. Then, the variations of the wave velocity and the attenuation coefficient of the body waves with the thermophysical parameters, such as the relaxation time (characterizing the flow-independent viscosity), thermal expansion coefficient of the soil particle and pore fluid, and the permeability coefficient (characterizing the flow-dependent viscosity) are discussed with some numerical examples.

2. Thermoviscoelastic Dynamic Model

In general, the volume change of viscoelastic materials is closely related to its elasticity and viscosity, that is, loading and time. For natural soil, its deformation under the action of external force is apparently time dependent, which exhibits obvious viscoelastic properties. In order to express the viscoelastic properties of natural soil, the present work introduced a linear viscoelastic model that is commonly employed to characterize materials' creep behavior, i.e., generalized Kelvin–Voigt model [33,34], which is composed of a spring in parallel with a dashpot, as illustrated in Figure 1.

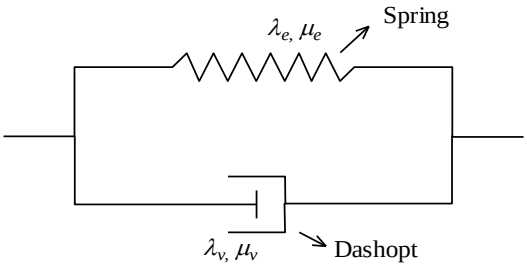

Figure 1. Generalized Kelvin–Voigt model.

The spring displayed in Figure 1 represents the material's linear-elastic response to the acting force, and the dashpot displayed in Figure 1 represents the material's damping behavior, and is employed to prevent the spring from reaching immediately to the applied force. The elastic constants of the material (denoted by λ_e and μ_e) are related to the viscosity constants (denoted by λ_v and μ_v) by the relaxation time (denoted by t_s) [35], which is written as:

$$\lambda_v = t_s\lambda_e,\ \mu_v = t_s\mu_e \tag{1}$$

where the relaxation time t_s characterizes the viscosity normalized with respect to the Lame elastic moduli and is assumed to be constant without loss of generality [31,32]. In the present work, the relaxation time t_s is utilized to determine the flow-independent viscosity from the solid skeleton.

It is assumed that the saturated soil is a kind of homogeneous and isotropic thermo-viscoelastic porous medium composed of the soil skeleton and pore fluid, and that the viscoelastic property of the soil skeleton may be simulated by the generalized Kelvin–Voigt model. According to the Biot theory, the motion equation for a unit total volume of biphase mixture in the absence of body force and dissipation can be expressed as [1,2]:

$$\sigma_{ij,j} = \rho\ddot{u}_i + \rho^w\ddot{w}_i \tag{2}$$

in which σ_{ij} denotes the total stress, and u_i and w_i represent the displacement of solid particles and the relative displacement of fluid in the direction i, respectively. $\rho = (1 - n^s)\rho^s + n^s\rho^w$ is the density of media, where n^s denotes the porosity, ρ^s represents the density of solid particle, and ρ^w designates the density of pore fluid.

Following the single stress state variable proposed by Bishop and Blight [2], the effective stress tensor σ'_{ij} can be described as:

$$\sigma'_{ij} = \sigma_{ij} + p_w\delta_{ij} \tag{3}$$

where δ_{ij} designates the Kronecker delta, and p_w designates the pore-fluid pressure.

According to the generalized thermoelastic theory, the compression of the solid skeleton is pore-fluid pressure and temperature variation dependent. Thus, the stress-strain relationship of the solid skeleton can be expressed as [36,37]:

$$\sigma'_{ij} = c^s_{ij}\left(\varepsilon_{ij} - \varepsilon^p_{ij} - \varepsilon^T_{ij}\right) \tag{4}$$

where c_{ij}^{s} designates the isotropic viscoelastic coefficient matrix of the solid skeleton. ε_{ij} denotes the strain tensor of the solid skeleton, ε_{ij}^{p} represents the strain tensor of the solid skeleton under the spherical tensor of the pore pressure, and ε_{ij}^{T} signifies the strain tensor of the solid skeleton under temperature variation.

The strain tensor of the solid skeleton can be expressed as:

$$\varepsilon_{ij} = \frac{1}{2}(u_{i,j} + u_{j,i}) \tag{5}$$

The strain tensor of the solid skeleton under the spherical tensor of liquid pressure, $\varepsilon_{\mathrm{ii}}^{p}$, can be expressed as:

$$\varepsilon_{11}^{p} = \varepsilon_{22}^{p} = \varepsilon_{33}^{p} = -\frac{1}{3K_s} p_w \tag{6}$$

where K_s denotes the compressibility moduli of the solid particles.

The strain tensor of the solid skeleton under the temperature variation, ε_{ij}^{T}, is written as:

$$\varepsilon_{ij}^{T} = a_c \theta \delta_{ij} \tag{7}$$

where a_c denotes the linear thermal expansion coefficient of the solid skeleton. $\theta = T - T_0$ designates the temperature variation from the reference temperature T_0 to the medium temperature T with the formula $|\theta / T_0| \ll 1$.

Substituting Equations (5)–(7) into Equation (4) and making algebraic operations yield:

$$\sigma'_{ij} = \left(\lambda_e + \lambda_v \frac{\partial}{\partial t}\right)\varepsilon_v \delta_{ij} + 2\left(\mu_e + \mu_v \frac{\partial}{\partial t}\right)\varepsilon_{ij} + \frac{K_b^s}{3K_s} p_w \delta_{ij} - K_b^s a_c \theta \delta_{ij} \tag{8}$$

in which

$$K_b^s = 3\lambda_e + 2\mu_e + (3\lambda_v + 2\mu_v)\frac{\partial}{\partial t} \tag{9}$$

where $\varepsilon_v = u_{i,i}$ designates the volumetric strain of the solid skeleton. λ_e and μ_e are the Lame elastic moduli of the solid skeleton. λ_v and μ_v are the shear and dilatant constants describing the flow-independent viscosity from the solid skeleton. It is worth noting herein that Equation (9) is the bulk modulus after considering the flow-independent viscosity associated with the solid skeleton, which is different from the convention in that the third term on the right of the formula is added to characterize the flow-independent viscosity.

For facilitating the writing of the symbols, let

$$\lambda_s = \lambda_e + \lambda_v \frac{\partial}{\partial t} \tag{10}$$

$$\mu_s = \mu_e + \mu_v \frac{\partial}{\partial t} \tag{11}$$

Substitution of Equation (8) in Equation (3) gives the total stress tensor of fluid-saturated soil as:

$$\sigma_{ij} = \lambda_s \varepsilon_v \delta_{ij} + 2\mu_s \varepsilon_{ij} - \alpha_s p_w \delta_{ij} - K_b^s a_c \theta \delta_{ij} \tag{12}$$

where $\alpha_s = 1 - K_b^s / 3K_s$.

Considering the compressibility of liquid in pores and solid grains, the constitutive model of the pore fluid under the effect of temperature variation for the thermoviscoelastic fluid-saturated media can be written as [28]:

$$p_w = M(\xi - \alpha_s \varepsilon_v + a_u \theta) \tag{13}$$

where $a_u = n^s a_w + (1 - n^s)a_s - (1 - \alpha_s)a_c$ is the thermal expansion coefficient of the thermoviscoelastic fluid-saturated media, in which a_s and a_w represent the linear thermal expansion coefficient of the solid particle and pore fluid, respectively. M is the Biot

modulus, $1/M = n^s/K_w + (1 - n^s)/K_s$, in which K_w denotes the volume modulus of pore fluid. $\xi = -w_{i,i}$ designates the relative strain of the pore fluid.

The flow equation of the liquid phase under a nonisothermal condition can be expressed as [28]:

$$-p_{w,i} = \rho^w \ddot{u}_i + (\rho^w/n^s)\ddot{w}_i + b\dot{w}_i + bD_T\theta_{,i} \tag{14}$$

where $b = \rho^w g/k_w$, in which k_w denotes the permeability coefficient and g represents the gravitational acceleration. D_T designates a phenomenological coefficient associated with the influence of the thermal gradient on the water flux.

The generalized non-Fourier heat conduction law proposed by Tzou [38,39] can be described by:

$$\left(1 + \tau_q \frac{\partial}{\partial t}\right) q_i = -K_T \left(1 + \tau_\theta \frac{\partial}{\partial t}\right) \nabla\theta \tag{15}$$

in which q_i is the heat flux. K_T is the thermal conductivity. τ_q and τ_θ denote the phase-lag of the heat flux and the temperature gradient, respectively.

Employing Equation (15), the heat conduction equation for fluid-saturated porous media can be written as:

$$K_T\left(\theta_{,ii} + \tau_\theta \dot{\theta}_{,ii}\right) = c_m\left(\dot{\theta} + \tau_q\ddot{\theta}\right) + K_b^s a_c T_0\left(\dot{\varepsilon}_v + \tau_q\ddot{\varepsilon}_v\right) - a_u T_0\left(\dot{p}_w + \tau_q\ddot{p}_w\right) \tag{16}$$

where $c_m = (1 - n^s)\rho^s c_s + n^s \rho^w c_w$ is the weight specific heat for fluid-saturated porous media, in which c_s and c_w denote the specific heat capacity of the solid grains and pore fluid, respectively. Equation (16) is the non-Fourier heat conduction equation that is derived from the double-phase lag model, which considers the influence of the phase-lag of the heat flux and temperature gradient that is employed, which can be coupled with the motion in Equations (12)–(14).

After incorporating Equations (2), (12)–(14), and (16), the wave equations in terms of displacement for thermoviscoelastic fluid-saturated medium can be yielded as:

$$\mu_e u_{i,jj} + a_1 u_{j,ji} + \mu_v \dot{u}_{i,jj} + a_2 \dot{u}_{j,ji} + a_3 \ddot{u}_{j,ji} + a_4 w_{j,ji} + a_5 \dot{w}_{j,ji} + a_6\theta_{,i} + a_7\dot{\theta}_{,i} + a_8\ddot{\theta}_{,i} = \rho\ddot{u}_i + \rho^w\ddot{w}_i \tag{17}$$

$$a_4 u_{j,ji} + a_5 \dot{u}_{j,ji} + M w_{j,ji} + a_9\theta_{,i} + a_{10}\dot{\theta}_{,i} = \rho^w\ddot{u}_i + (\rho^w/n^s)\ddot{w}_i + b\dot{w}_i \tag{18}$$

$$\begin{aligned} &a_6 T_0\left(\dot{u}_i + \tau_q\ddot{u}_i\right)_{,i} + a_7 T_0\left(\ddot{u}_i + \tau_q\dddot{u}_i\right)_{,i} + a_8 T_0\left(\dddot{u}_i + \tau_q\ddddot{u}_i\right)_{,i} + M v_1 T_0\left(\dot{w}_i + \tau_q\ddot{w}_i\right)_{,i} + \\ &a_{10} T_0\left(\ddot{w}_i + \tau_q\dddot{w}_i\right)_{,i} + a_{11}\left(\dot{\theta} + \tau_q\ddot{\theta}\right) + a_{12}\left(\ddot{\theta} + \tau_q\dddot{\theta}\right) + a_{13}\left(\dddot{\theta} + \tau_q\ddddot{\theta}\right) = -K_T\left(\theta + \tau_\theta\dot{\theta}\right)_{,ii} \end{aligned} \tag{19}$$

with

$$a_1 = \lambda_e + \mu_e + \alpha_e^2 M$$

$$a_2 = \lambda_v + \mu_v - 2\alpha_e\alpha_v M$$

$$a_3 = \alpha_v^2 M$$

$$a_4 = \alpha_e M$$

$$a_5 = -\alpha_v M$$

$$a_6 = \alpha_e v_1 M - (3\lambda_e + 2\mu_e)a_c$$

$$a_7 = \alpha_v v_2 M - (3\lambda_v + 2\mu_v)a_c$$

$$a_8 = -\alpha_v^2 M a_c$$

$$a_9 = M v_1 - bD_T$$

$$a_{10} = \alpha_v M a_c$$

$$a_{11} = v_1^2 M T_0 - c_m$$

$$a_{12} = 2\alpha_{10} v_1 T_0$$

$$a_{13} = \alpha_v^2 a_c^2 M T_0$$
$$v_1 = (1-\alpha_e)a_c - n^s a_w - (1-n^s)a_s$$
$$v_2 = (2\alpha_e - 1)a_c + n^s a_w + (1-n^s)a_s$$
$$\alpha_e = 1 - (3\lambda_e + 2\mu_e)/3K_s$$
$$\alpha_v = (3\lambda_v + 2\mu_v)/3K_s$$

3. Wave Field Solution of Body Waves

In thermoviscoelastic saturated soil, body waves include compression, thermal, and shear waves, and propagate inside an unbounded domain. The diagram of wave field motion of body waves in soil half-space is displayed in Figure 2. As illustrated in Figure 2, the compression and thermal waves, a kind of propulsive wave, propagate along the particle vibration direction. The shear wave, caused by rotating external force and generated under shear deformation, propagates along the route perpendicular to the vibration direction of the particle.

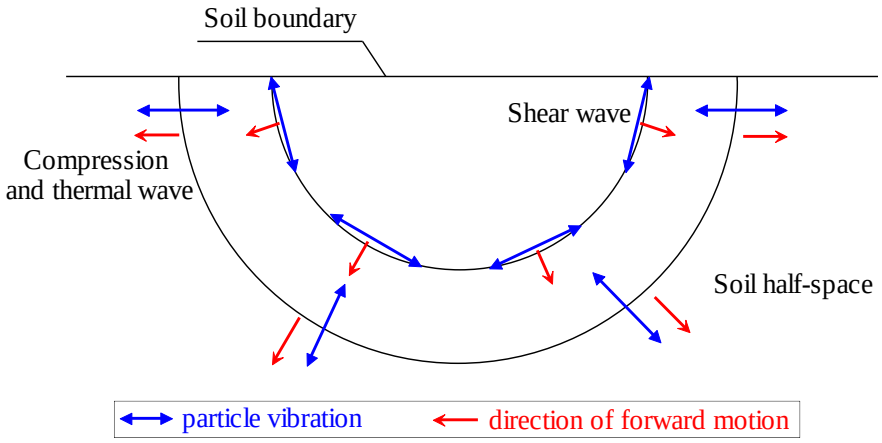

Figure 2. Diagram of wave field motion of body waves.

According to Helmholtz vector decomposition principle, the vector field can be replaced as the sum of the gradient of the scalar field (φ_s and φ_w) and the curl of the vector field (ψ_s and ψ_w):

$$\boldsymbol{u} = \nabla\varphi_s + \nabla \times \boldsymbol{\psi}_s \tag{20}$$
$$\boldsymbol{w} = \nabla\varphi_w + \nabla \times \boldsymbol{\psi}_w \tag{21}$$

where the two sets symbols, φ_s, φ_w and ψ_s, ψ_w, denote the scalar potential and vector potential of the solid skeleton and pore fluid, respectively.

Substituting Equations (20) and (21) into Equations (17)–(19) and making divergence and curl operations yield

$$(a_1+\mu_e)\nabla^2\varphi_s + (a_2+\mu_v)\nabla^2\dot{\varphi}_s + a_3\nabla^2\ddot{\varphi}_s + a_4\nabla^2\varphi_w + a_5\nabla^2\dot{\varphi}_w + a_6\theta + a_7\dot{\theta} + a_8\ddot{\theta} = \rho\ddot{\varphi}_s + \rho^w\ddot{\varphi}_w \tag{22}$$
$$a_4\nabla^2\varphi_s + a_5\nabla^2\dot{\varphi}_s + M\nabla^2\varphi_w + a_9\theta + a_{10}\dot{\theta} = \rho^w\ddot{\varphi}_s + (\rho^w/n^s)\ddot{\varphi}_w + b\dot{\varphi}_w \tag{23}$$
$$\begin{aligned} &a_6T_0\nabla^2(\dot{\varphi}_s + \tau_q\ddot{\varphi}_s) + a_7T_0\nabla^2(\ddot{\varphi}_s + \tau_q\dddot{\varphi}_s) + a_8T_0\nabla^2(\dddot{\varphi}_s + \tau_q\ddddot{\varphi}_{si}) + Mv_1T_0\nabla^2(\dot{\varphi}_w + \tau_q\ddot{\varphi}_w) + \\ &a_{10}T_0\nabla^2(\ddot{\varphi}_w + \tau_q\dddot{\varphi}_w) + a_{11}\left(\dot{\theta} + \tau_q\ddot{\theta}\right) + a_{12}\left(\ddot{\theta} + \tau_q\dddot{\theta}\right) + a_{13}(\ddot{\theta} + \tau_q\ddddot{\theta}) = -K_T\nabla^2\left(\theta + \tau_\theta\dot{\theta}\right) \end{aligned} \tag{24}$$
$$\rho\ddot{\boldsymbol{\psi}}_s + \rho^w\ddot{\boldsymbol{\psi}}_w = \mu_e\nabla^2\boldsymbol{\psi}_s + \mu_v\nabla^2\dot{\boldsymbol{\psi}}_s \tag{25}$$
$$\rho^w\ddot{\boldsymbol{\psi}}_s + (\rho^w/n^s)\ddot{\boldsymbol{\psi}}_w + b\dot{\boldsymbol{\psi}}_w = 0 \tag{26}$$

The potentials of solid phase, liquid phase, and temperature variation when the body waves propagate in the fluid-saturated soil can be expressed as:

$$\varphi_s = A_s \mathrm{e}^{\mathrm{i}(\omega t - k_p \boldsymbol{r})},\ \varphi_w = A_w \mathrm{e}^{\mathrm{i}(\omega t - k_p \boldsymbol{r})},\ \theta = A_T \mathrm{e}^{\mathrm{i}(\omega t - k_p \boldsymbol{r})} \tag{27}$$

$$\boldsymbol{\psi}_s = \boldsymbol{B}_s \mathrm{e}^{\mathrm{i}(\omega t - k_s \boldsymbol{r})},\ \boldsymbol{\psi}_w = \boldsymbol{B}_w \mathrm{e}^{\mathrm{i}(\omega t - k_s \boldsymbol{r})} \tag{28}$$

where A_s, A_w, A_T, $\boldsymbol{B}_s$, and $\boldsymbol{B}_w$ stand for the amplitudes of corresponding potential; $\mathrm{i} = \sqrt{-1}$ denotes the imaginary unit; $\omega = 2\pi f$ designates the angular frequency in which f represents the frequency; k_p and k_s signify the complex wavenumber of the compressional wave including thermal wave and shear wave, respectively; $\boldsymbol{r}$ is the position vector.

The following formulas can be yielded by substituting Equations (27) and (28) into Equations (22)–(26) and making some algebraic operations as:

$$\begin{pmatrix} p_{11} & p_{12} & p_{13} \\ p_{21} & p_{22} & p_{23} \\ p_{31} & p_{32} & p_{33} \end{pmatrix} \begin{pmatrix} A_s \\ A_w \\ A_T \end{pmatrix} = \begin{pmatrix} 0 \\ 0 \\ 0 \end{pmatrix} \tag{29}$$

$$\begin{pmatrix} s_{11} & s_{12} \\ s_{21} & s_{22} \end{pmatrix} \begin{pmatrix} \boldsymbol{B}_s \\ \boldsymbol{B}_w \end{pmatrix} = \begin{pmatrix} 0 \\ 0 \end{pmatrix} \tag{30}$$

with

$$p_{11} = \rho\omega^2 + \left[a_3\omega^2 - (a_2 + \mu_v)\mathrm{i}\omega - (a_1 + \mu_e)\right]k_p^2$$

$$p_{12} = \rho^w\omega^2 - (a_4 + a_5\mathrm{i}\omega)k_p^2$$

$$p_{13} = a_6 + a_7\mathrm{i}\omega - a_8\omega^2$$

$$p_{21} = \rho^w\omega^2 - (a_4 + a_5\mathrm{i}\omega)k_p^2$$

$$p_{22} = \rho^w\omega^2/n^s - b\mathrm{i}\omega - Mk_p^2$$

$$p_{23} = a_9 + a_{10}\mathrm{i}\omega$$

$$p_{31} = \omega T_0 k_p^2\left[a_7\omega\left(1 + \tau_q\mathrm{i}\omega\right) + \left(a_8\omega^2 - a_6\right)\left(\mathrm{i} - \tau_q\omega\right)\right]$$

$$p_{32} = \omega T_0 k_p^2\left[a_{10}\omega\left(1 + \tau_q\mathrm{i}\omega\right) - Mv_1\left(\mathrm{i} - \tau_q\omega\right)\right]$$

$$p_{33} = \omega\left(a_{11} - a_{13}\omega^2\right)\left(\mathrm{i} - \tau_q\omega\right) - a_{12}\omega^2\left(1 + \tau_q\mathrm{i}\omega\right) - K_T k_p^2(1 + \tau_\theta\mathrm{i}\omega)$$

$$s_{11} = \rho\omega^2 - (\mu_e + \mu_v\mathrm{i}\omega)k_s^2$$

$$s_{12} = \rho^w\omega^2$$

$$s_{21} = \rho^w\omega^2$$

$$s_{22} = (\rho^w/n^s)\omega^2 - b\mathrm{i}\omega$$

At last, the characteristic equation for body waves in thermoviscoelastic fluid-saturated medium is obtained

$$\begin{vmatrix} p_{11} & p_{12} & p_{13} \\ p_{21} & p_{22} & p_{23} \\ p_{31} & p_{32} & p_{33} \end{vmatrix} = 0 \tag{31}$$

$$\begin{vmatrix} s_{11} & s_{12} \\ s_{21} & s_{22} \end{vmatrix} = 0 \tag{32}$$

where Equation (31) is the dispersion equation for compression and thermal waves, and Equation (32) is the dispersion equation of shear wave.

The following two formulas can be derived from formulas (31) and (32), respectively, by implementing the determinant operation as:

$$e_1 k_p^6 + e_2 k_p^5 + e_3 k_p^4 + e_4 k_p^3 + e_5 k_p^2 + e_6 k_p + e_7 = 0 \tag{33}$$

$$e_8 k_s^2 + e_9 = 0 \tag{34}$$

where the coefficients e_1–e_7 and e_8–e_9 can be expressed as the combination of the elements p_{11}–p_{33} in Equation (31) and the elements s_{11}–s_{22} in Equation (32) respectively, in which the specific forms of these coefficients are not given herein. Considering the attenuation of the amplitudes for the body waves along its propagation direction, Equation (33) has only three meaningful complex roots, i.e., $k_p = \mathrm{Re}(k_p) + \mathrm{iIm}(k_p)$, two of which stand for the complex wavenumbers of the compression waves (typically signed as P_1 and P_2 waves in descending order of phase velocity), whereas the third of which stands for the complex wavenumber of the thermal wave (typically signed as T wave). Likewise, Equation (34) has only one meaningful complex root, i.e., $k_s = \mathrm{Re}(k_s) + \mathrm{iIm}(k_s)$, which is the complex wavenumber of the shear wave (typically signed as S wave).

In general, the wave velocity and attenuation coefficient of P_1, P_2, T, and S waves can be defined as:

$$v_{p1} = \frac{\omega}{\mathrm{Re}(k_{p1})},\ v_{p2} = \frac{\omega}{\mathrm{Re}(k_{p2})},\ v_T = \frac{\omega}{\mathrm{Re}(k_{p3})},\ v_s = \frac{\omega}{\mathrm{Re}(k_s)} \tag{35}$$

$$\delta_{p1} = \mathrm{Im}(k_{p1}),\ \delta_{p2} = \mathrm{Im}(k_{p2}),\ \delta_T = \mathrm{Im}(k_{p3}),\ \delta_s = \mathrm{Im}(k_s) \tag{36}$$

where the two sets of symbols, v_{p1}, v_{p2}, v_T, v_s and δ_{p1}, δ_{p2}, δ_T, δ_s represent the wave velocity and attenuation coefficient of P_1, P_2, T, and S waves, respectively.

4. Calculation Examples and Parametric Analysis

In order to study the propagation behavior of body waves in the thermoviscoelastic fluid-saturated ground, this section utilizes calculation examples to discuss the effect of various thermophysical parameters of the thermoviscoelastic fluid-saturated medium on wave velocity and the attenuation coefficient of each body wave. In the present work, the values of thermophysical parameters refer to the values selected in Table 1 [28] unless otherwise specified. Figure 3 highlights the thermophysical parameters utilized for sensitivity analysis of wave velocity and attenuation coefficient of body waves in thermoviscoelastic soil. In this work, the influences of frequency, relaxation time, permeability coefficient, thermal expansion coefficient of solid particle and water, phase-lag of heat flux and temperature gradient, and thermal conductivity on the wave velocity and attenuation coefficient of body waves were the main object of study.

To verify the correctness of the above derivation, the results of this paper were compared with those obtained by Yang et al. [40] without considering the nonflowing viscosity of the saturated soil solid skeleton. The values of the relevant soil parameters were taken as: $n^s = 0.05 \sim 0.45$, $\rho^s = 2650\ \mathrm{kg/m^3}$, $\rho^w = 1000\ \mathrm{kg/m^3}$, $K_s = 36$ GPa, $K_w = 2$ Gpa, $k_w = 10^{-5}$ m/s, $\mu_e = 26.1$ Mpa, $K_b^s = 43.6$ Mpa, and $f = 100$ Hz, $t_s = 0$ s. Figure 4 shows the comparison curves of P_1, P_2, and S waves with the porosity of saturated soil. It can be seen from Figure 4 that the wave velocity of the P_1 wave in saturated soil gradually decreased nonlinearly and the wave velocity of the S wave increased approximately linearly as the porosity of the soil increased, whereas the wave velocity of the P_2 wave was almost unaffected. It can also be seen that the results obtained from the calculations in this paper are in good qualitative and quantitative agreement with those of Yang et al. [40], which can indicate the correctness of the theoretical derivation and the validity of the paper's calculation results.

Table 1. Thermoviscoelastic parameters of fluid-saturated soil for calculation examples.

Parameters/Symbol	Value/Unit	Parameters/Symbol	Value/Unit
Porosity n^s	0.4	Thermal conductivity of soil K_T	2.2 J/s/m/K
Density of solid grain ρ^s	2650 kg/m^3	Specific heat of solid grain c_s	937 J/kg/K
Density of water ρ^w	820 kg/m^3	Specific heat of water c_w	4186 J/kg/K
Bulk modulus of solid grain K_s	35 GPa	Initial temperature T_0	300 K
Bulk modulus of water K_w	2 GPa	Thermo-osmosis D_T	2.7×10^{-11} m^2/s/K
Lame constant λ_e	1.2×10^8 Pa	Volume thermal expansion of soil a_c	3.0×10^{-5} K^{-1}
Lame constant μ_e	2.6×10^7 Pa	Thermal expansion of solid grain a_s	3.0×10^{-5} K^{-1}
Permeability coefficient k_w	1.0×10^{-4} m/s	Thermal expansion of water a_w	3.0×10^{-4} K^{-1}
Relaxation time t_s	0.5×10^{-3} s	Phase-lag of heat flux τ_q	2.0×10^{-2} s
Frequency f	50 Hz	Phase-lag of temperature gradient τ_θ	1.5×10^{-2} s

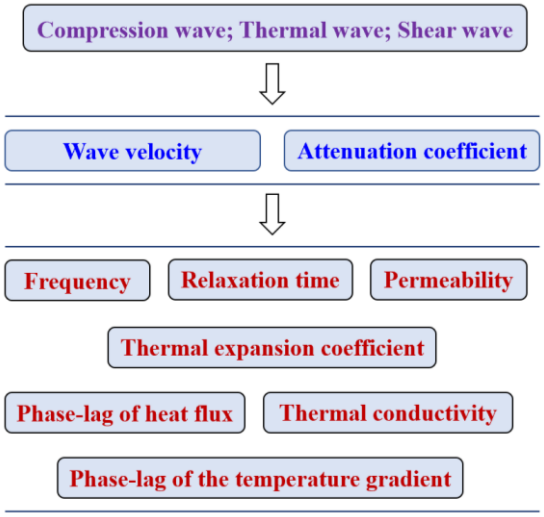

Figure 3. Diagram of parametric analysis for body waves.

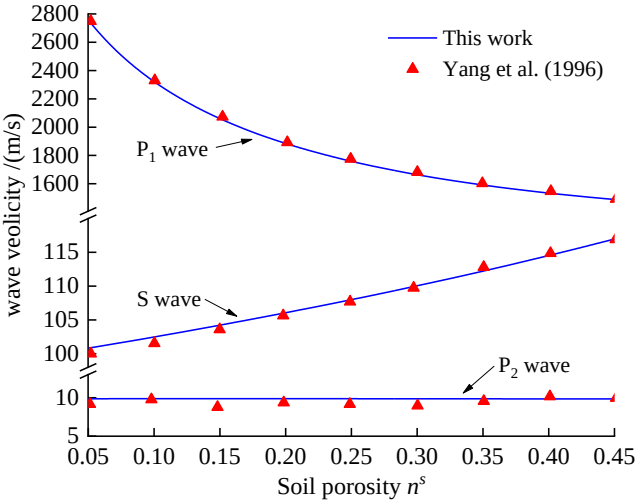

Figure 4. Comparison curve of the wave velocity of body waves for various values of the soil porosity.

The dependency of the wave velocity and the attenuation coefficient of body waves on the relaxation time t_s and frequency f are depicted in Figures 5 and 6. The frequency ranged from 0.01 Hz to 150 Hz therein. The relaxation time associated with the flow-independent viscosity was taken to be 0 s, 5×10^{-4} s, and 1×10^{-3} s, respectively.

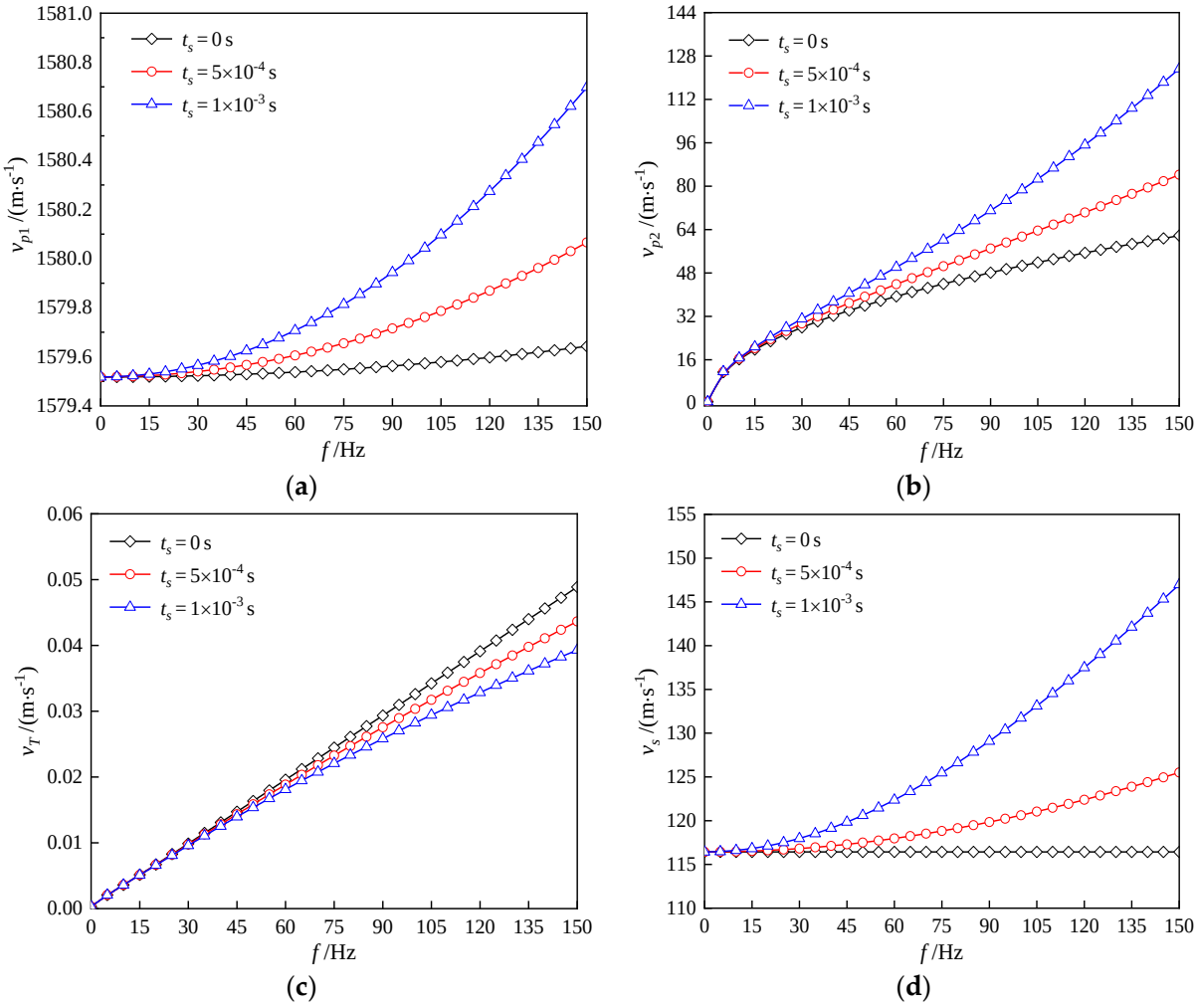

Figure 5. Wave velocities of body waves for various values of the relaxation time and frequency. (**a**) P_1 wave, (**b**) P_2 wave, (**c**) T wave and (**d**) S wave.

As depicted in Figure 5, the wave velocity of the P_1 wave was the largest, followed by the S wave, and then the P_2 wave, whereas the wave velocity of the thermal wave was the smallest. More importantly, Figure 5a,b,d show that although the wave velocities of P_1, P_2, and S waves all increased with the increase of relaxation time t_s, the influence of relaxation time t_s on the wave velocity of P_1 wave was unnoticeable compared with its influence on the other waves. Whereas Figure 5c shows that the wave velocity of the thermal wave will decrease with the increase of relaxation time t_s. In other words, under the frequency condition herein, the positive relativities between the wave velocity of P_1, P_2, and S waves and the frequency f gradually increased with the relaxation time t_s increasing; however, the positive relativity of the thermal wave gradually decreased with the relaxation time t_s increasing.

The enlargement of relaxation time t_s increased the wave velocity of P_1, P_2, and S waves and decreased the wave velocity of the thermal wave, as illustrated in Figure 5. At the same time, Figure 6 shows that the attenuation coefficient of the thermal wave was the largest, followed by the P_2 wave, and then the S wave, whereas the attenuation coefficient of the P_1 wave was the smallest. The variation trends of the attenuation coefficient of P_1, P_2, and the S waves with the frequency f were basically the same as their wave velocity trends. However, the attenuation coefficient of the thermal wave had a different variation with and without considering the relaxation time accounting for flow-independent viscosity. The attenuation coefficient of the thermal wave increased rapidly at first, then gradually stabilized and remained constant when the relaxation time was not considered, i.e., $t_s = 0$,

and then slightly reduced when the relaxation time was considered, i.e., $t_s \neq 0$ herein, in which the greater the relaxation time, the more prominent the decreasing trend of the attenuation coefficient of thermal wave.

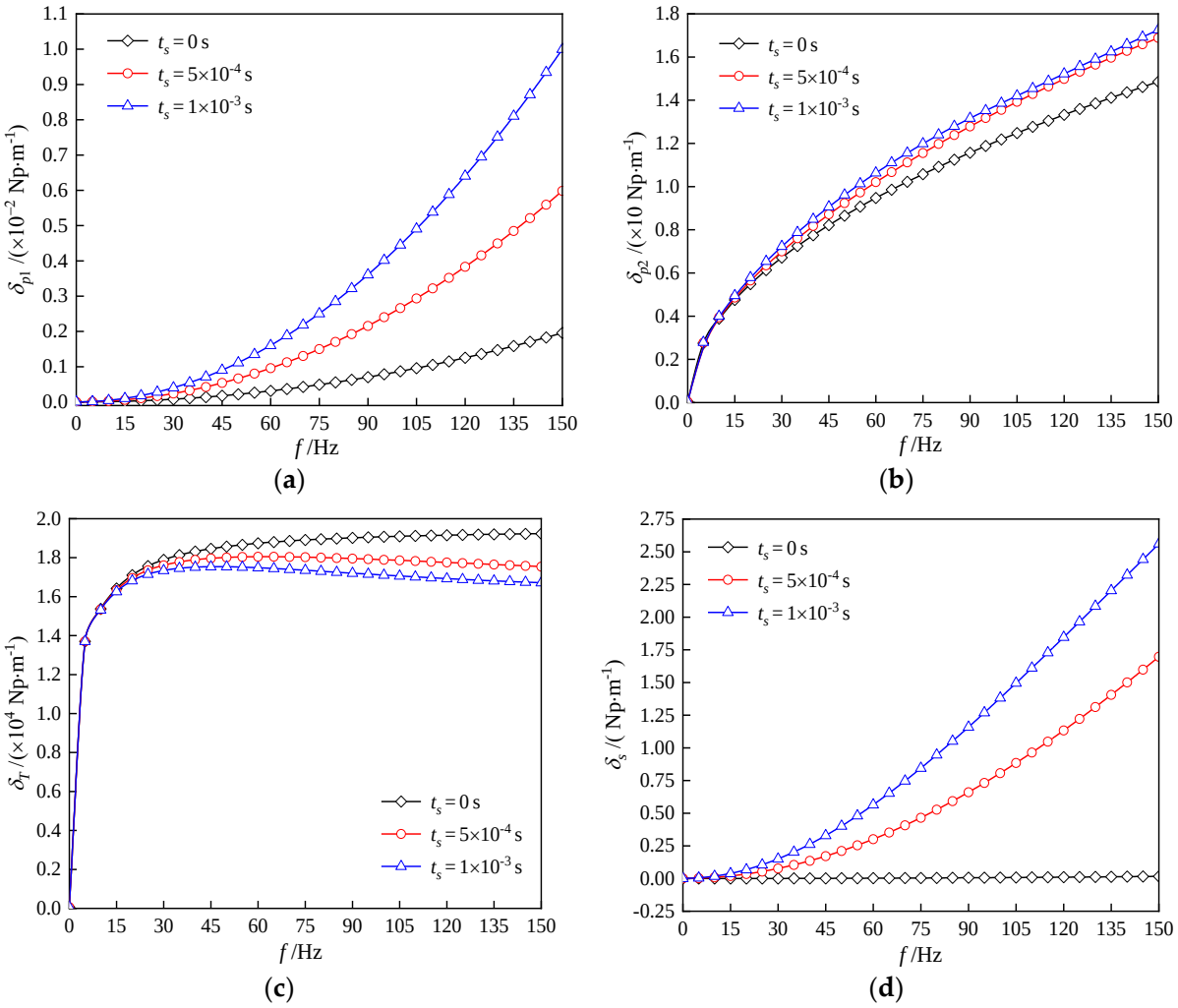

Figure 6. Attenuation coefficients of body waves for various values of the relaxation time and frequency. (**a**) P_1 wave, (**b**) P_2 wave, (**c**) T wave and (**d**) S wave.

The relationships of thermal expansion coefficients of solid particle and pore fluid and the wave velocity and attenuation coefficient of body waves are portrayed in Figures 7 and 8 when $t_s = 0.5 \times 10^{-4}$ s. The thermal expansion coefficients of solid particle and pore fluid all ranged from 0.0 K^{-1} to 1.0×10^{-3} K^{-1}. The enlargement of the thermal expansion coefficient of solid particle was accompanied by the increase of both wave velocity and the attenuation coefficient for the P_1 wave, whereas the augmentation of the thermal expansion coefficient of pore fluid was accompanied by the increase of wave velocity and the decrease of the attenuation coefficient for the P_1 wave, as depicted in Figures 7a and 8a. Meanwhile, a diminution of the thermal expansion coefficient of the solid particle resulted in a negative growth of wave velocity and a positive growth of the attenuation coefficient for the P_2 wave, whereas the influence of the thermal expansion coefficient of pore fluid on the P_2 wave was quite contrary, as displayed in Figures 7b and 8b.

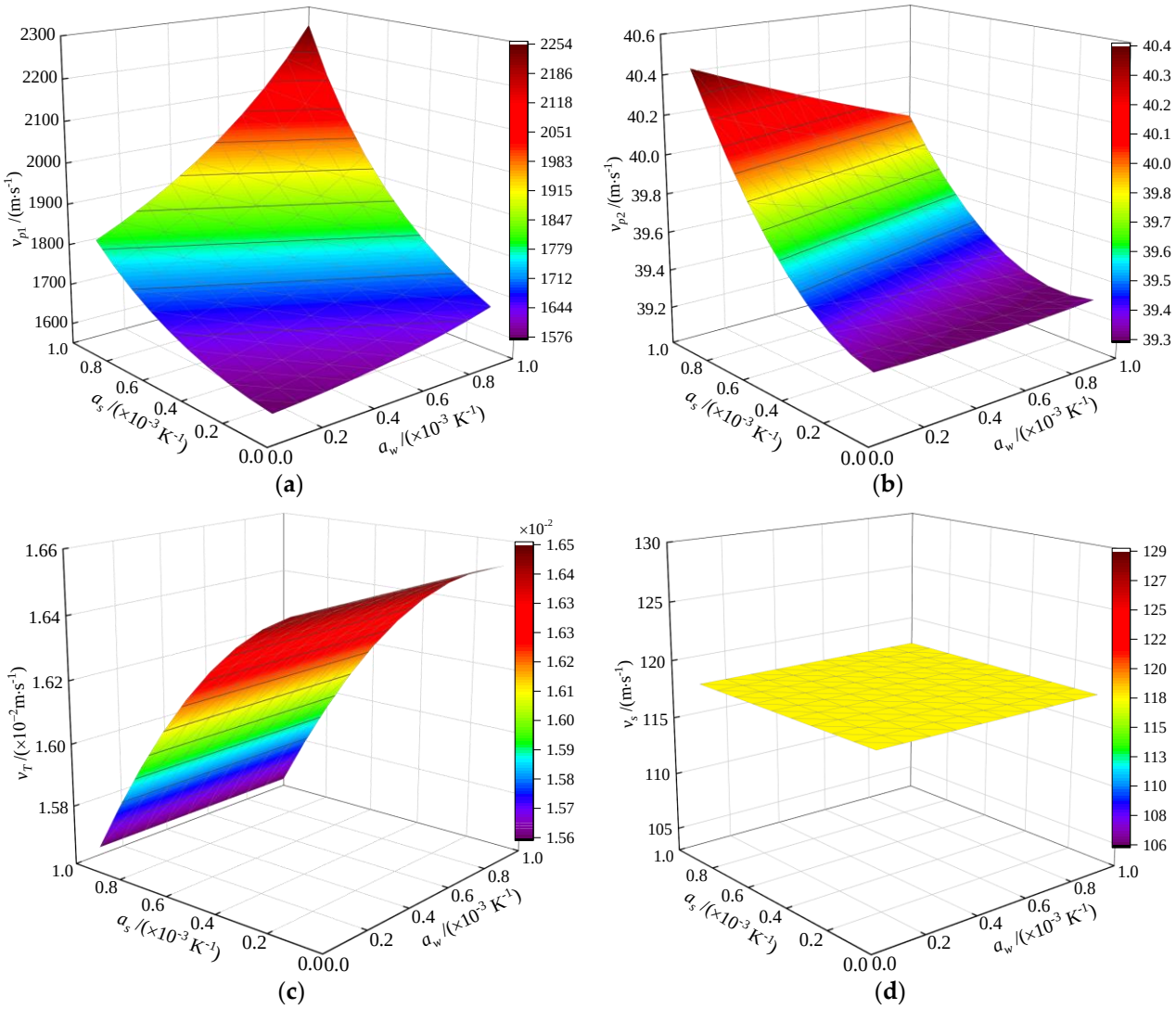

Figure 7. Wave velocities of body waves for various values of the thermal expansion coefficient of the solid particle and pore fluid. (**a**) P_1 wave, (**b**) P_2 wave, (**c**) T wave and (**d**) S wave.

In addition, Figures 7d and 8d present that the wave velocity and attenuation coefficient of the S wave are independent on the change in the thermal expansion coefficients of the solid particle and pore fluid, which can also be obtained legibly by Equations (32) and (34). Lastly, the dependency of the wave velocity and attenuation coefficient of the thermal wave on the thermal expansion coefficient is presented in Figures 7c and 8c, which is not repeated herein because the thermal wave had a very small wave velocity (about $1/10^5$ of v_{p1}) and a very fast attenuation (about 10^5 times δ_{p1}) that is difficult to measure in practice.

The flow-dependent viscosity of the fluid-saturated soil is characterized by the parameter b shown in Equation (14), where b is expressed as the ratio of the product of the fluid density ρ^w and gravitational acceleration g to the permeability coefficient k_w. Apparently, the flow-dependent viscosity of the fluid-saturated soil was finally represented by the permeability coefficient k_w. In this work, the permeability coefficient k_w ranged from 10^{-6} m/s to 1 m/s, which included common soil types such as normal-consolidation/overconsolidation clay and dense/loose sand. The permeability coefficient of 1 m/s was selected in this work only to make the discussion convenient. The actual permeability coefficient of the oil was much smaller than 1 m/s. Figures 9 and 10 demonstrate the effects of the permeability coefficient k_w and relaxation time t_s on the wave velocity and attenuation coefficient of P_1, P_2, and S waves. As mentioned above, the thermal wave had

slow velocity and fast attenuation which are difficult to measure in practice; thus, the effect of the permeability coefficient on its dispersion behavior will not be discussed herein.

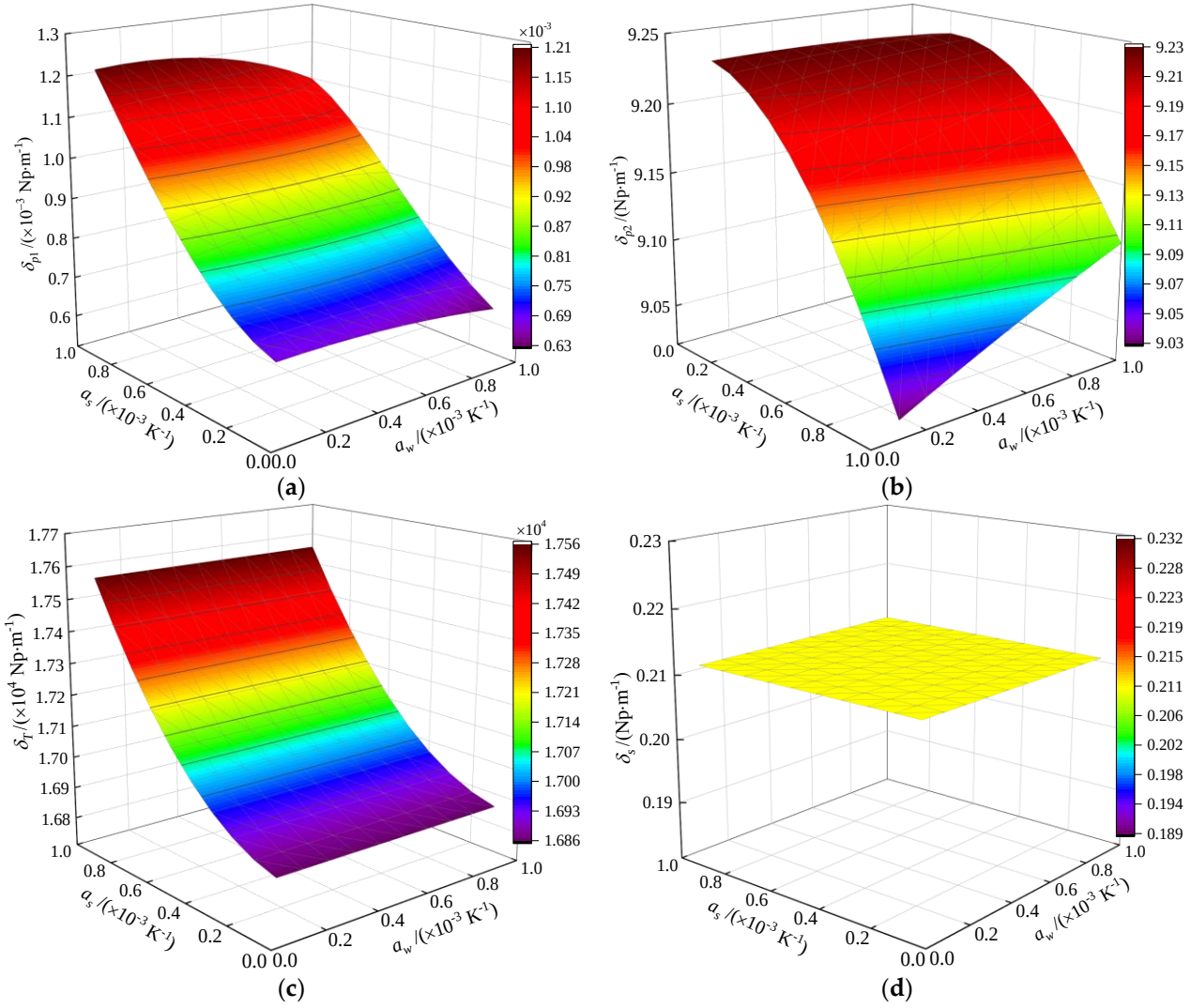

Figure 8. Attenuation coefficients of body waves for various values of the thermal expansion coefficient of the solid particle and pore fluid. (**a**) P_1 wave, (**b**) P_2 wave, (**c**) T wave and (**d**) S wave.

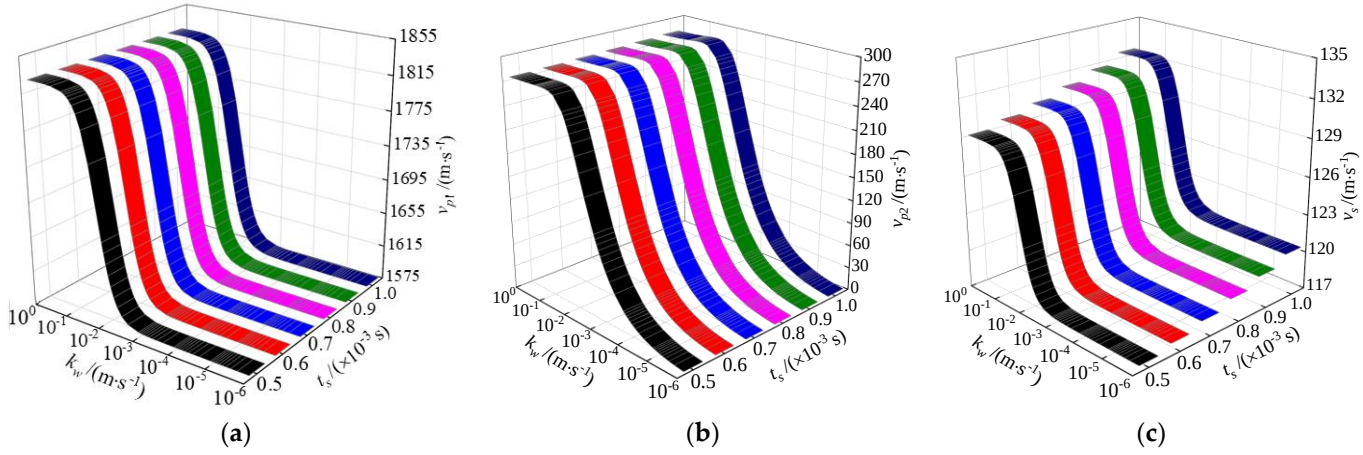

Figure 9. Wave velocities of body waves for various values of the permeability coefficient under different relaxation times. (**a**) P_1 wave, (**b**) P_2 wave, (**c**) S wave.

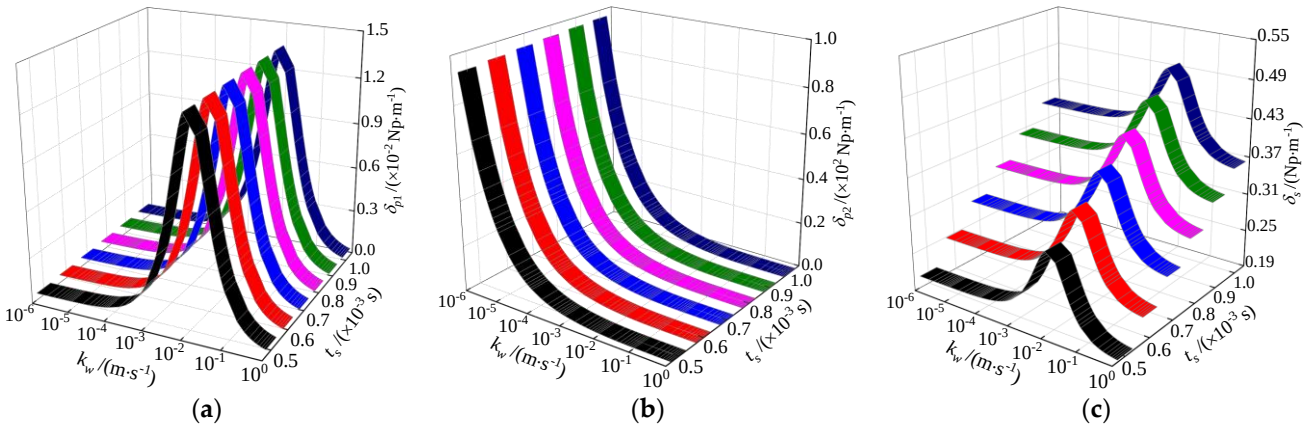

Figure 10. Attenuation coefficients of body waves for various values of the permeability coefficient under different relaxation times. (**a**) P_1 wave, (**b**) P_2 wave, (**c**) S wave.

From Figure 9a,c, it can be captured that the wave velocities of the P_1 and S waves remained constant in the high zone (k_w= 0.1 ∼ 1 m/s) and low zone (k_w= 10^{-6}∼ 10^{-3} m/s) of the permeability coefficient, whereas they increased rapidly with the augmentation of the permeability coefficient in the middle permeability zone (k_w= 10^{-3}∼ 10^{-1} m/s). The difference was that the wave velocity of the P_2 wave increased sharply with the increase of the permeability coefficient in the low and middle permeability zones (k_w= 10^{-6}∼ 10^{-1} m/s) and remained constant in the high permeability zone (k_w= 0.1 ∼ 1 m/s), as illustrated in Figure 9b. Furthermore, Figure 9 shows that the increase of relaxation time t_s made the dependence curves of the wave velocity of P_1, P_2, and S waves on the permeability coefficient k_w move upward (in the positive direction of the vertical coordinate), in which the upward movement of the S wave curve was the most obvious, followed by the P_2 wave, and the least obvious was the P_1 wave. The influence law of relaxation time shown in Figure 9 corresponds to that in Figure 5.

As shown in Figure 10a,c the variation of the attenuation coefficients of the P_1 and S waves were an approximately normal distribution over the whole permeability zone. However, with the augmentation of the permeability coefficient k_w, the attenuation coefficient of the P_2 wave first decreased rapidly, then decreased tardily, and then finally tended to be steady. Similarly, the greater the relaxation time t_s, the more the curves of attenuation coefficients of the P_1, P_2, and S waves moved upward.

In addition to the influence of thermophysical parameters such as relaxation time, frequency, thermal expansion coefficient of the solid particle and pore fluid, and the permeability coefficient in the preceding discussion, the authors found that the change in the thermal conductivity, phase-lag of the heat flux, and phase-lag of the temperature gradient had little effect on the dispersion behavior of P1, P2, and S waves, which can almost be ignored. However, the change in these parameters had a great influence on the dispersion behavior of the thermal wave, as presented in Figures 11 and 12. Due to limited space, the current study will not elaborate on it. It should be noted that the above theoretical study can be further proven by a nondestructive testing technique [41–44].

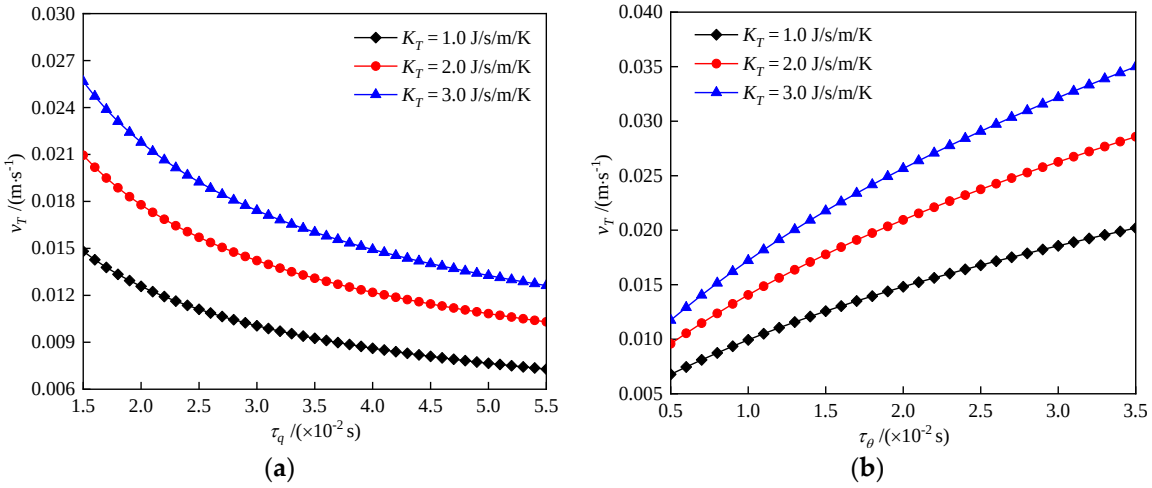

Figure 11. Wave velocity of the thermal wave for different values of the phase-lag and thermal conductivity. (**a**) phase-lag of the heat flux, (**b**) phase-lag of the temperature gradient.

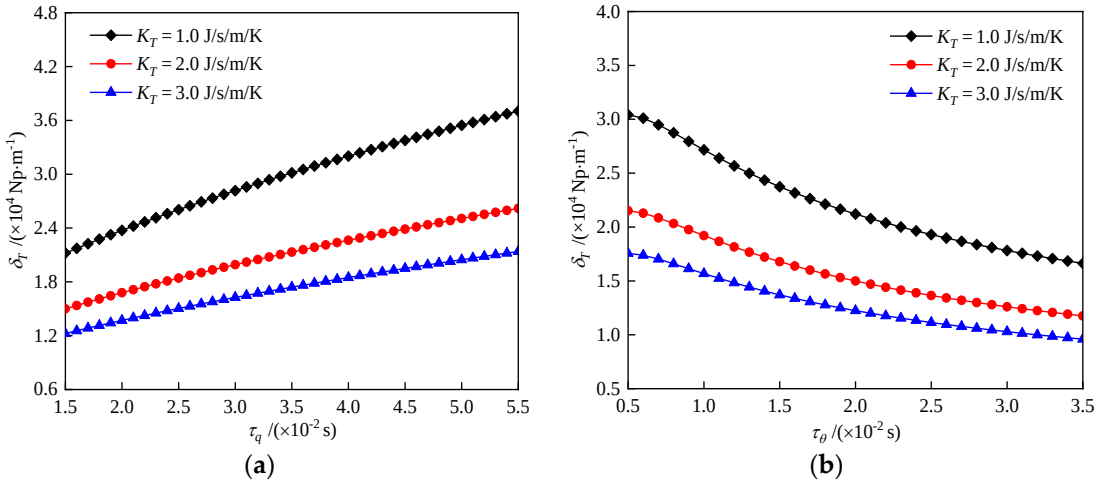

Figure 12. Attenuation coefficient of the thermal wave for different values of the phase-lag and thermal conductivity. (**a**) phase-lag of the heat flux, (**b**) phase-lag of the temperature gradient.

5. Conclusions

In this work, the influences of flow-independent viscosity of the soil skeleton and the thermal effect on elastic waves were considered, and then the propagation characteristics of body waves in thermoviscoelastic fluid-saturated ground were studied. The calculation examples were employed to calculate the wave velocity and attenuation coefficient of each wave and analyzed the influence of the thermophysical parameters. The main conclusions obtained from the parametric analysis are as follows:

1. The flow-independent viscosity of the soil had a great influence on the propagation behavior of each body wave, which cannot be ignored.
2. The propagation behavior of the P_1 and P_2 waves was related to the thermal expansion coefficient of the solid particle and pore fluid, whereas the S wave was almost independent.
3. The permeability coefficient and frequency had important influences on the propagation of body waves.

The conclusions found in this work had certain guiding significance for related research and engineering application.

Author Contributions: Theoretical analysis, validation, writing, B.W.; Writing and translation, X.Z.; Check, B.S. All authors have read and agreed to the published version of the manuscript.

Funding: The work described in this paper was supported by the National Natural Science Foundation of China (Grant No. 51978320), Gansu Province Qingyang City Scientific Support Funds (Grant No. QY2021A-F028, QY2021A-F029).

Institutional Review Board Statement: Not applicable.

Informed Consent Statement: Not applicable.

Data Availability Statement: The data supporting the results reported in the paper can be accessed from the corresponding authors.

Acknowledgments: The findings and opinions expressed in this article are only those of the authors and do not necessarily reflect the views of the sponsors.

Conflicts of Interest: The authors declare no conflict of interest.

References

1. Biot, M.A. Theory of Propagation of Elastic Waves in a Fluid-Saturated Porous Solid. I. Low-Frequency Range. *J. Acoust. Soc. Am.* **1956**, *28*, 168–178. [CrossRef]
2. Biot, M.A. Theory of propagation of elastic waves in a fluid-saturated porous solid. II. Higher frequency range. *J. Acoust. Soc. Am.* **1956**, *28*, 179–191. [CrossRef]
3. Plona, T.J. Observation of a second bulk compressional wave in a porous medium at ultrasonic frequencies. *Appl. Phys. Lett.* **1980**, *36*, 259–261. [CrossRef]
4. Berryman, J.G. Confirmation of Biot's theory. *Appl. Phys.Lett.* **1980**, *37*, 382–384. [CrossRef]
5. Jones, J.P. Rayleigh waves in a porous, elastic, saturated solid. *J. Acoust. Soc. Am.* **1961**, *33*, 959–962. [CrossRef]
6. Hajra, S.; Mukhopadhyay, A. Reflection and refraction of seismic waves incident obliquely at the boundary of a liquid-saturated porous solid. *Bull. Seismol. Soc. Am.* **1982**, *72*, 1509–1533. [CrossRef]
7. Sharma, M.; Gogna, M. Wave propagation in anisotropic liquid-saturated porous solids. *J. Acoust. Soc. Am.* **1991**, *90*, 1068–1073. [CrossRef]
8. Carcione, J.M. Wave propagation in anisotropic, saturated porous media: Plane-wave theory and numerical simulation. *J. Acoust. Soc. Am.* **1996**, *99*, 2655–2666. [CrossRef]
9. Berryman, J.G. Fluid effects on shear waves in finely layered porous media. *Geophysics* **2005**, *70*, N1–N15. [CrossRef]
10. Wang, D.; Wang, L.; Ding, P. The effects of fracture permeability on acoustic wave propagation in the porous media: A microscopic perspective. *Ultrasonics* **2016**, *70*, 266–274. [CrossRef]
11. Zhou, F.; Ma, Q. Propagation of Rayleigh waves in fluid-saturated non-homogeneous soils with the graded solid skeleton distribution. *Int. J. Numer. Anal. Methods Geomech.* **2016**, *40*, 1513–1530. [CrossRef]
12. Ciarletta, M.; Straughan, B.; Tibullo, V. Acceleration waves in a nonlinear Biot theory of porous media. *Int. J. Non-Linear Mech.* **2018**, *103*, 23–26. [CrossRef]
13. Xiong, F.; Sun, W.; Liu, J. The stability of poro-elastic wave equations in saturated porous media. *Acta Geophys.* **2021**, *69*, 65–75. [CrossRef]
14. Tung, D.X. Surface waves in nonlocal transversely isotropic liquid-saturated porous solid. *Arch. Appl. Mech.* **2021**, *91*, 2881–2892. [CrossRef]
15. Zhang, S.; Yan, D.; Wang, Y.; Wang, Y.; Laude, V. Wave propagation in one-dimensional fluid-saturated porous phononic crystals with partial-open pore interfaces. *Int. J. Mech. Sci.* **2021**, *195*, 106227. [CrossRef]
16. Rohan, E.; Nguyen, V.-H.; Naili, S. Homogenization approach and Floquet-Bloch theory for wave analysis in fluid-saturated porous media with mesoscopic heterogeneities. *Appl. Math. Model.* **2021**, *91*, 1–23. [CrossRef]
17. Du, Q.Z.; Liu, L.L.; Sun, J.B. Numerical modeling of seismic wavefield in anisotropic viscoelastic porous medium with the pseudo-spectral method. *Acta Phys.Sin.* **2007**, *56*, 6143–6149.
18. Zhou, F.; Zhao, W.; Cao, Y. Numerical simulation of elastic wave field in gas-saturated and water-saturated porous media. *Chin. J. Solid Mech.* **2015**, *36* (Suppl. S1), 152–159.
19. Liu, H.; Zhou, F.; Zhang, R.; Yue, G. Effects of thermoelastic coupling on the propagation of body waves in saturated porous media. *Chin. J. Rock Mech. Eng.* **2020**, *39* (Suppl. S1), 2693–2702.
20. Liu, H.; Zhou, F.; Hao, L. Reflection of Plane S Waves at the Boundary of Saturated Porous Thermo-Elastic Media. *China Earthq. Eng. J.* **2021**, *43*, 105–112.
21. Diallo, M.S.; Appel, E. Acoustic wave propagation in saturated porous media: Reformulation of the Biot/Squirt flow theory. *J. Appl. Geophys.* **2000**, *44*, 313–325. [CrossRef]
22. Singh, B. On propagation of plane waves in generalized porothermoelasticity. *Bull. Seismol. Soc. Am.* **2011**, *101*, 756–762. [CrossRef]

23. La Ragione, L.; Recchia, G.; Jenkins, J. Wave propagation in an unconsolidated granular material: A micro-mechanical approach. *Wave Motion* **2020**, *99*, 102653. [CrossRef]
24. Liu, J.; Cui, Z.; Sevostianov, I. Effect of stresses on wave propagation in fluid-saturated porous media. *Int. J. Eng. Sci.* **2021**, *167*, 103519. [CrossRef]
25. Biot, M.A. Thermoelasticity and irreversible thermodynamics. *J. Appl. Phys.* **1956**, *27*, 240–253. [CrossRef]
26. Lord, H.W.; Shulman, Y. A generalized dynamical theory of thermoelasticity. *J. Mech. Phys. Solids* **1967**, *15*, 299–309. [CrossRef]
27. Youssef, H. Theory of generalized porothermoelasticity. *Int. J. Rock Mech. Min. Sci.* **2007**, *44*, 222–227. [CrossRef]
28. Liu, G.; Xie, K.; Ye, R. Mode of a spherical cavity's thermo-elastodynamic response in a saturated porous medium for non-torsional loads. *Comput. Geotech.* **2010**, *37*, 381–390. [CrossRef]
29. Zhou, F.; Liu, H.; Cai, Y. Analysis of propagation characteristics of Rayleigh waves in saturated porothermoelastic media. *Rock Soil Mech.* **2020**, *41*, 315–324.
30. Bardet, J.P. A Viscoelastic Model for the Dynamic Behavior of Saturated Poroelastic Soils. *J. Appl. Mech.* **1992**, *59*, 128–135. [CrossRef]
31. Militano, G.; Rajapakse, R. Dynamic response of a pile in a multi-layered soil to transient torsional and axial loading. *Geotechnique* **1999**, *49*, 91–109. [CrossRef]
32. Xie, K.-H.; Liu, G.-B.; Shi, Z.-Y. Dynamic response of partially sealed circular tunnel in viscoelastic saturated soil. *Soil Dyn. Earthq. Eng.* **2004**, *24*, 1003–1011. [CrossRef]
33. Sills, G.C.; Wheeler, S.J.; Thomas, S.D.; Gardner, T.N. Behaviour of offshore soils containing gas bubbles. *Geotechnique* **1991**, *41*, 227–241. [CrossRef]
34. Cheng, Z.; Leong, E.C. Finite element simulations of wave propagation in soils using a Viscoelastic model. *Soil Dyn. Earthq. Eng.* **2016**, *88*, 207–214. [CrossRef]
35. Michaels, P. In situ determination of soil stiffness and damping. *J. Geotech. Geoenviron. Eng.* **1998**, *124*, 709–719. [CrossRef]
36. Ieşan, D. On a theory of thermoviscoelastic materials with voids. *J. Elast.* **2011**, *104*, 369–384. [CrossRef]
37. Sharma, K.; Kumar, P. Propagation of plane waves and fundamental solution in thermoviscoelastic medium with voids. *J. Therm. Stresses* **2013**, *36*, 94–111. [CrossRef]
38. Tzou, D.Y. A Unified Field Approach for Heat Conduction From Macro- to Micro-Scales. *J. Heat Transf.* **1995**, *117*, 8–16. [CrossRef]
39. Tzou, D.Y. Experimental support for the lagging behavior in heat propagation. *J. Thermophys. Heat Transf.* **1995**, *9*, 686–693. [CrossRef]
40. Yang, J.; Wu, S.; Cai, Y. Characteristics of propagation of elastic waves in saturated soils. *J. Vib. Eng.* **1996**, *9*, 128–137.
41. Wang, H.; Chen, H.; Chen, C.; Zhang, H.; Jiang, H.; Song, T.; Feng, S. The Structural Performance of CFRP Composite Plates Assembled with Fiber Bragg Grating Sensors. *Symmetry* **2021**, *13*, 1631. [CrossRef]
42. Wang, H.; Feng, S.; Gong, X.; Guo, Y.; Xiang, P.; Fang, Y.; Li, Q. Dynamic performance detection of CFRP composite pipes based on quasi-distributed optical fiber sensing techniques. *Front. Mater. Struct. Mater.* **2021**, *8*, 285. [CrossRef]
43. Wang, H.; Song, T.; Yan, J.; Xiang, P.; Feng, S.; Hui, D. Improved analytical method for interfacial-slip control design of steel-concrete composite structures. *Symmetry* **2021**, *13*, 1225. [CrossRef]
44. Sasy Chan, Y.W.; Wang, H.P.; Xiang, P. Optical Fiber Sensors for Monitoring Railway Infrastructures: A Review towards Smart Concept. *Symmetry* **2021**, *13*, 2251. [CrossRef]